



This is a repository copy of *Induced p-type semi-conductivity in yttria-stabilised zirconia*.

White Rose Research Online URL for this paper:

<https://eprints.whiterose.ac.uk/145994/>

Version: Submitted Version

---

**Article:**

Vendrell, X. and West, A.R. [orcid.org/0000-0002-5492-2102](https://orcid.org/0000-0002-5492-2102) (2019) Induced p-type semi-conductivity in yttria-stabilised zirconia. *Journal of the American Ceramic Society*, 102 (10). pp. 6100-6106. ISSN 0002-7820

<https://doi.org/10.1111/jace.16492>

---

This is the pre-peer reviewed version of the following article: Vendrell, X, West, AR. Induced p-type semiconductivity in yttria-stabilized zirconia. *J Am Ceram Soc.* 2019, which has been published in final form at <https://doi.org/10.1111/jace.16492>. This article may be used for non-commercial purposes in accordance with Wiley Terms and Conditions for Use of Self-Archived Versions.

**Reuse**

Items deposited in White Rose Research Online are protected by copyright, with all rights reserved unless indicated otherwise. They may be downloaded and/or printed for private study, or other acts as permitted by national copyright laws. The publisher or other rights holders may allow further reproduction and re-use of the full text version. This is indicated by the licence information on the White Rose Research Online record for the item.

**Takedown**

If you consider content in White Rose Research Online to be in breach of UK law, please notify us by emailing [eprints@whiterose.ac.uk](mailto:eprints@whiterose.ac.uk) including the URL of the record and the reason for the withdrawal request.



[eprints@whiterose.ac.uk](mailto:eprints@whiterose.ac.uk)  
<https://eprints.whiterose.ac.uk/>

# Induced *p*-type semi-conductivity in yttria-stabilised zirconia

Xavier Vendrell and Anthony R. West

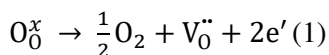
Department of Materials Science and Engineering, University of Sheffield, Mappin Street, Sheffield, S13JD, United Kingdom.

## Abstract

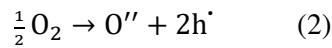
8 mol% yttria-stabilised zirconia, 8YSZ, ceramic is an oxide ion conductor at atmospheric pressure but shows the onset of *p*-type semi-conduction, in addition to the pre-existing oxide ion conduction, on application of a *dc* bias in the range 4 – 66 Vcm<sup>-1</sup> and at temperatures in the range 150 – 750 °C. **The *p*-type behaviour is attributed to the location and hopping of holes on oxygen.** This contrasts with the commonly-observed introduction of *n*-type conduction under reducing conditions and high fields. The hole conductivity increases with both *dc* bias and *p*O<sub>2</sub>. Its **occurrence** may contribute to the early stages of flash **phenomena in 8YSZ ceramics.**

## Introduction

Yttria-stabilised zirconia (YSZ) shows high oxide ion conduction at elevated temperatures and is one of the most important ceramic electrolytes in solid oxide cells (SOCs)<sup>1,2</sup>. YSZ shows high chemical and thermal stability at high temperatures, without degradation, in contact with the anode or cathode in SOC<sup>3,4</sup>. The electrolytic domain of YSZ is very wide and extends in reducing atmospheres down to a *p*O<sub>2</sub> value of ~10<sup>-20</sup> atm<sup>5</sup>. At lower *p*O<sub>2</sub>, the onset of *n*-type electronic conduction occurs<sup>6</sup> and is associated with loss of oxygen from the ceramic, which can be described using Kröger-Vink notation as, ideally:



At higher *p*O<sub>2</sub>, YSZ is certainly stable to ~1 atm of O<sub>2</sub>; the possible onset of *p*-type conduction at higher *p*O<sub>2</sub> is not well-established, mainly due to the difficulty of performing conductivity measurements at high oxygen partial pressure. Nevertheless, in the *p*-type region it is assumed that the reverse of mechanism (1) would occur by the idealised reaction:



It was shown recently that electronic conduction can be introduced into Y-doped  $\text{ZrO}_2$  under the action of a small *dc* bias at high temperature<sup>7,8</sup>. Similar conductivity increases had been observed in other acceptor-doped systems such as Mg- or Zn-doped  $\text{BaTiO}_3$  perovskite<sup>9-12</sup> but in those cases, the conductivity was also sensitive to  $p\text{O}_2$  in the surrounding atmosphere, from which it was possible to determine that the carriers were *p*-type. As far as we are aware, there are no reports on the possible sensitivity of the conductivity of 8YSZ to higher values of  $p\text{O}_2$ .

It was assumed, but not proven, that the electronic conductivity introduced into 8YSZ under a small *dc* bias was *p*-type<sup>7</sup>. In a typical test **using two terminal impedance measurements to study the effect of *dc* bias on electrical properties, the impedance response is expected to be different at the two electrodes**. At the positive electrode (anode) **where the oxygen reduction reaction (ORR)** mobile electrons and reduction in associated *n*-type conductivity or to ionisation of redox-active elements in the sample and a possible increase in associated *p*-type conductivity. In the ceramics literature, it is widely assumed, but rarely proven, that the redox-active elements responsible for *p*-type conductivity are unavoidable impurities such as Fe, **but** recent results on doped titanate perovskites point to under-bonded oxide ions as the source and location of holes<sup>9-11</sup>.

At the negative electrode, **where the oxygen evolution reaction (OER) occurs**, electrons may be injected into the sample as a consequence, for instance, of oxygen loss, leading to *n*-type conductivity.

In practice, one or other of these two possible electrode processes may dominate in response to a *dc* bias, or both may occur simultaneously. As yet, there are no well-established guidelines on the response of samples, **at the two electrodes**, to a small *dc* bias, although at higher fields, irreversible changes are likely to commence once the effective decomposition potential of the sample is exceeded.

In considering the effects of varying  $p\text{O}_2$  in the atmosphere surrounding a sample, the explanation of any change in electrical properties should be clear since a single, uniform response across a

sample surface is expected to occur. This allows an unambiguous identification of *n*- or *p*-type behaviour in the case of extrinsic conductivity or indeed, of intrinsic behaviour if no conductivity changes are detected.

In the studies on acceptor-doped BaTiO<sub>3</sub><sup>9-11</sup>, atmosphere tests indicated *p*-type behaviour and therefore, it was concluded that the *dc* bias-induced changes responsible for enhanced *p*-type conductivity were dominated by reactions at the anode. For 8YSZ, the question remains open since, although Y<sup>3+</sup> (with lower formal charge than Zr<sup>4+</sup>) may be regarded as an acceptor dopant, giving rise to under-bonded oxygen ions and possible *p*-type behaviour, it is also clear that YSZ can lose oxygen under highly reducing conditions leading to *n*-type behaviour. Studies on the grain size distribution in YSZ ceramics subjected to high constant voltage or current at 1300 °C in an atmosphere of 5% H<sub>2</sub> were interpreted in terms of a non-linear distribution in oxygen potential through the sample, allowing observation of the cathodic and anodic regions from a discontinuity in grain sizes<sup>13</sup>.

In recent years, the flash sintering (FS) technique has been developed as a consequence of simultaneously exposing solid materials to high voltage and heat<sup>14-16</sup>. FS has attracted much attention due to the dramatic decrease of furnace sintering temperature and the short times needed to obtain high density materials. Following its discovery using powders, ceramics and single crystals of YSZ<sup>17,18</sup>, it has been used to sinter a wide range of materials<sup>19-22</sup>. The mechanisms that occur during flash are still under debate, although certainly, samples show a dramatic increase of both temperature and conductivity during the flash event and less dramatically, in a premonitory period before the onset of flash. The increase in conductivity is electronic in nature and the associated increase in sample temperature is attributed to Joule heating<sup>19,23-27</sup>; what is unclear is whether additional changes in intrinsic properties of the material occur in response to the bias, leading to an enhanced Joule heating effect, rapid sintering and associated luminescence; **there is debate as to whether electroluminescence occurs<sup>28</sup> or whether the observed luminescence is caused by black body radiation<sup>29</sup>.**

The aim of the present work work has been to investigate further the effect of both atmosphere and a small *dc* bias, simultaneously, on the electrical properties of 8YSZ.

## Experimental

8YSZ (99.9 %, Sigma-Aldrich) powders, without added binder, were pressed uniaxially at 200 MPa and fired at 1550 °C for 5 h in air, with heating and cooling rates of 5 °C/min. Pellet dimensions were ~6 mm diameter, ~2 mm thickness and densities were  $\geq 97$  %.

For electrical property measurements, electrodes were fabricated by the application of Pt paste to opposite pellet faces, which was dried and hardened at 900 °C for 2 h. Samples, with their electrodes stuck to strips of Pt foil, were attached to the Pt leads of an in-house conductivity jig and their impedance measured using an Agilent 4294A impedance analyser over the frequency range 40 Hz to 3 MHz with an *ac* voltage of 0.1 V. Isothermal impedance measurements were made in flowing N<sub>2</sub>, air or O<sub>2</sub>, with *p*O<sub>2</sub> values of approx. 10<sup>-2</sup>, 0.2 and 1 atm., respectively, over the temperature range 150 to 750 °C. For selected temperatures, a small *dc* bias, in the range 1-16 V, was applied across the sample at the same time as impedance measurements were made. The small applied voltages corresponded to voltage gradients of ~ 4-66 Vcm<sup>-1</sup>.

Impedance data were corrected for the blank cell capacitance, the series jig resistance, the pellet thickness and electrode contact area. Therefore, resistance and capacitance data are reported using resistivity and permittivity units of  $\Omega$  cm and F cm<sup>-1</sup>, respectively. Corrected data were analysed and modelled using Zview (Scriber Associates Inc.) software.

## Results and Discussion

Since it is well-known that YSZ may suffer from blackening when exposed to high electric fields<sup>30</sup>, preliminary tests were made to see the effect of an applied *dc* bias at 658 °C on the appearance of ceramic samples. Results are shown in Figure 1. With an applied bias of 16 V (~70 V/cm), sample A shows no sign of coloration of pellet surfaces **after cooling the pellets to room temperature**. With 19 V bias (~80 V/cm), **however**, sample B shows a mild-yellow coloration which is not uniformly present across the pellet surfaces. With 24 V bias (~100 V/cm), sample C

shows obvious blackening, some of which extends through the ceramic interior of fractured sections (not shown).

Blackening of YSZ has been reported on several occasions previously, although it is also widely recognised that it is not easy to reduce 8YSZ<sup>30-32</sup>. A number of investigations have been performed to clarify the nature of the blackened material, most of them at room temperature, but the chemical nature of blackened zirconia is unclear and is still under discussion<sup>33-36</sup>, although specific blackening at the cathode has been identified<sup>29</sup>. Since evidence of coloration and blackening was seen with applied voltages of 18-24 V, impedance measurements were made with lower voltages, in the range 1 to 16 V, to reduce possible influence of sample reduction. However, the possibility of sample reduction during impedance measurements at a combination of high temperatures, >750 °C and low voltages, < 16V cannot be discarded. **An explanation for blackening is given<sup>29</sup> in which blackening commences at the cathode, extends to cover the whole sample and then largely disappears on removal of the bias after flash. The results shown in Figure 1c are consistent with the occurrence of the blackening seen in 8YSZ single crystals, but showed some residual black spots at the end of the experiment.**

Impedance data for 8YSZ ceramic, measured in air, are shown in Figure 2 as  $Z^*$  complex plane plots at two temperatures, 430 and 558 °C (inset). An *ac* signal of nominally 100 mV was used for initial, zero-bias impedance measurements. Subsequently, a *dc* bias of up to 16 V was applied and the impedance measurements repeated after a lapse of 10 minutes to allow samples to equilibrate and impedance values to reach **an approximate** steady state. Finally, the *dc* bias was removed and the impedance measurements repeated.

With no *dc* bias, the impedance complex plane plot at 430 °C shows three features, Figure 2: a partial arc at high frequency attributed to the bulk response, a second arc at intermediate frequency attributed to the grain boundary and an inclined spike at low frequency attributed to the sample-electrode-air interface. Resistance values of the bulk,  $R_b$ , and grain boundary,  $R_{gb}$ , were obtained from the intercepts on the real,  $Z'$  impedance axis. The total sample resistance, obtained from either the sum of  $R_b$  and  $R_{gb}$  or the intercept of the spike on the  $Z'$  axis, had a value of ~10 k $\Omega$

cm. At 558 °C (inset), the impedance data were similar to those at 430 °C, but, due to the increase of temperature and with the limitations of the available frequency range used, a separate value for the bulk response was not observed. The total resistance had a value of  $\sim 900 \Omega \text{ cm}$ .

Impedance data were strongly sensitive to a small *dc* bias, in the range 1-16 V, Figure 2; similar behaviour has already been observed for Y-rich compositions in the  $\text{ZrO}_2\text{-Y}_2\text{O}_3$  system<sup>8</sup>. Application of a *dc* bias had two effects on the impedance data: (i) the total impedance shifted to lower resistances, whilst maintaining the overall features of the complex plane plots and (ii) the low frequency spike collapsed drastically to give a small depressed arc. Both effects were fully reversible on removal of the *dc* bias, as shown in Figure 2. The decrease in total resistance was voltage-dependent at both temperatures, but was more pronounced at higher temperature.

The effect of 12 V *dc* bias on total sample resistance at 558 °C in the three atmospheres of  $\text{N}_2$ , air and  $\text{O}_2$  is shown in Figure 3. The system was allowed to stabilise for 1 hour in each atmosphere before impedance data were collected on application of a *dc* bias. In each atmosphere, the total sample resistance decreased rapidly before levelling off but required several minutes to reach a steady state resistance; in  $\text{O}_2$ , in particular, approximately 25 minutes were required to reach a steady state. The resistance decrease was greater with increasing  $p\text{O}_2$  and is therefore attributed to an increase in hole concentration. On removal of the bias, in each atmosphere the sample fully recovered its original resistance value within a few minutes.

These impedance data indicate that a *dc* bias induces electronic conduction in 8YSZ, which therefore becomes a mixed conductor. Transport number data for holes and oxide ions in the mixed conducting region were obtained from fits of impedance data to the equivalent circuits shown in Figure 4. In the absence of *dc* bias, impedance data fitted well the circuit shown in (a) which contains series-connected bulk, grain boundary and electrode-sample contact impedances. Fits are shown for one example in (a); residuals between experimental and fitted data are shown in (c).

In order to model the effect of a *dc* bias and the introduction of an electronic conduction pathway in parallel with the ionic conduction, additional resistances were placed in parallel with sample and electrode resistances in the equivalent circuit, (b). It was clear from both the collapse of the electrode spike and the reduction in overall resistance that these modifications to the equivalent circuit were necessary. A resistance  $R_e$  was placed in parallel with both bulk and grain boundary impedances to represent electronic conduction in YSZ; a second resistor,  $R_{w,e}$ , was connected in parallel with the sample-electrode constant phase element (CPE) to model the finite *dc* resistance at the electrode interface, as shown in (b). The value for  $R_e$  was obtained from the reduction in sample resistance that occurred on application of the *dc* bias.

The electronic transport number,  $t_e$ , is given by the relation,  $t_e = \sigma_e / (\sigma_e + \sigma_i)$ , where  $\sigma_e = 1/R_e$  and  $\sigma_i = 1/(R_b + R_{gb})$ . Transport number data are summarised in Figure 5 for measurements in three atmospheres at 558 °C as a function of applied bias. It can be seen that, for instance, the electronic transport number increased from  $t_e = 0$ , at 0 V/cm bias to values in the range 0.5 to 0.7 depending on  $pO_2$  with a bias of 16 V (66 V/cm).

These results demonstrate clearly that 8YSZ becomes a *p*-type mixed conductor on application of a small *dc* bias. Because it is *p*-type, the main changes under these conditions that have influenced the conductivity are focused on the anode region. The only realistic location of holes in 8YSZ is on oxygen; in practice, a hole on oxygen in a crystal lattice may be regarded as an  $O^-$  ion. In order to create holes on lattice oxide ions, a requirement is that those particular oxide ions should ionise readily.

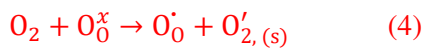
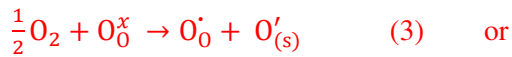
An essential feature of the  $O^{2-}$  ion that helps to explain easy hole creation is that, whereas the  $O^{2-}$  ion is thermodynamically unstable in the gas phase, it is stabilised in crystal lattices by the increased lattice energy associated with divalent  $O^{2-}$  ions compared with that for (hypothetical) structures containing monovalent  $O^-$  ions. Consequently,  $O^{2-}$  ions in a crystal lattice that are at sample surfaces, grain boundaries, or in local defect environments in which they are surrounded by an effective positive charge of less than  $2+$ , may be regarded as under-bonded. Depending on the degree of under-bonding, they may either ionise readily in response to increasing  $pO_2$  or a *dc*



bias or ionise spontaneously without the need for an external stimulus. It appears that, for 8YSZ, a simple change in  $pO_2$  alone is insufficient to ionise under-bonded oxide ions whereas this can be achieved by application of a  $dc$  bias. However, previous studies on Y-rich YSZ compositions<sup>8</sup> showed that with increasing Y content, such as in 50YSZ,  $p$ -type conduction could be introduced by increasing  $pO_2$  as well as with a  $dc$  bias.

The effect of  $pO_2$  and  $dc$  bias on the electronic conductivity of 8YSZ may be interpreted using Figure 6. 8YSZ is, of course, an oxide ion conductor whose properties, when it is used as the electrolyte in SOCs, are in the electrolytic domain. But, with increasing  $pO_2$  and at the same time as a  $dc$  bias is applied, YSZ gradually enters the  $p$ -type domain, giving rise to the observed mixed oxide ion /  $p$ -type conduction.

The effect of increasing  $pO_2$  alone (max. 1 atm.) is insufficient to introduce significant levels of  $p$ -type semiconductivity in 8YSZ, but with an applied bias, the electronic conductivity increases, Figure 2 and the increase is greater with increasing  $pO_2$ , Figure 3. Equation (2) indicates one simple case of how gas phase  $O_2$  molecules may adsorb on sample surfaces, dissociate and ionise to form  $O^{2-}$  ions; other possibilities include formation of peroxide ions  $O_2^{2-}$  and superoxide ions,  $O_2^-$  by a similar mechanism, but without dissociation of the  $O_2$  molecules. Since holes on lattice oxide ions are created by this process, as evidenced by the increased  $p$ -type conductivity, equation (2) may be extended to include singly-ionised lattice oxide ions as the hole location sites, with for instance either surface  $O^-$  ions or superoxide ions as the product derived from the gas phase, as follows:



Note that, although we use Kröger-Vink notation to indicate the site location and formal charge on species that occupy regular lattice sites, it is unclear how the formal charge on surface species should be represented; we therefore specify the expected free ion charges for the surface species shown in equations (3) and (4). Since it is proposed that only partial oxidation of under-bonded

lattice oxide ions occurs, it is also probably more realistic that the gas phase oxygen molecules are only partly reduced in the process, equations (3,4), rather than fully reduced as in equation (2).

The changes in conductivity on applying or removing a *dc* bias, Figure 3, are not instantaneous. The processes indicated by equations (3,4) are initiated by, but are not limited to, reactions at the sample-gas interface; they also involve changes in the oxygen stoichiometry of the sample interior, especially at longer times. These changes are clearly distinct from those associated with the oxygen loss that may occur under severely reducing conditions, which would lead to reduction in sample oxygen content and *n*-type behaviour. The conditions under which the two possible types of oxygen non-stoichiometry occur in practice remain to be resolved.

Since the onset of *p*-type conduction is the response first seen on application of a small *dc* bias that does not exceed the practical decomposition potential of YSZ, it is tempting to conclude that this also represents the first step in the increased conductivity associated with flash sintering. This may be true for YSZ, but a wide range of other materials can also be flash-sintered, many of which may be *n*-type prior to application of a bias. However, additional components of the flash sintering process remain to be identified, in particular, at the temperatures and voltages used in typical flash experiments (750 °C, 150 V/cm)<sup>17</sup> which are higher than those used here (558 °C, 50 V/cm). Thus, it was shown that the temperature of onset of flash sintering 3YSZ and an associated rapid increase in its conductivity both increased with increasing  $pO_2$ <sup>24</sup>. The implication was that oxygen loss and the creation of negative electronic charge carriers were responsible, in contrast to the present report of enhanced *p*-type conductivity with increasing  $pO_2$ <sup>24</sup>.

## Conclusions

8YSZ is an oxide ion conductor under normal conditions of use at atmospheric pressure, but on application of a small *dc* bias during impedance measurements, it becomes a mixed conductor due to the introduction of *p*-type semiconductivity. The *p*-type behaviour appears to be associated with uptake and possible dissociation of oxygen molecules at the sample-positive electrode

interface where the oxygen atoms or molecules pick up electrons from underbonded  $O^{2-}$  ions to form  $O^-$  species, which are equivalent to holes trapped on oxygen. The resulting hole conductivity increases with both *dc* bias and  $pO_2$  and leads to an increase in Joule heating of the sample which may contribute to the early stage in flash sintering 8YSZ.

## Acknowledgements

This project received funding from the European Union's Horizon 2020 research and innovation programme under the Marie Skłodowska-Curie grant agreement No 700786.

## References

- 1 Boudghene, A., and Traversa E. Solid oxide fuel cells (SOFCs): a review of an environmentally clean and efficient source of energy. *Renew Sustain Energy Rev* 2002; **6**: 433–455.
- 2 Fergus JW. Electrolytes for solid oxide fuel cells. *J Power Sources* 2006; **162**: 30–40.
- 3 Maskell WC, Steele BCH. Solid state potentiometric oxygen gas sensors. *J Appl Electrochem* 1986; **16**: 475–489.
- 4 Kharton V, Marques F, Atkinson A. Transport properties of solid oxide electrolyte ceramics: a brief review. *Solid State Ionics* 2004; **174**: 135–149.
- 5 Park J-H, Blumenthal RN. Electronic Transport in 8 Mole Percent  $Y_{2}O_{3}$ - $ZrO_{2}$ . *J Electrochem Soc* 1989; **136**: 2867.
- 6 Park J-H, Blumenthal RN. Electronic Transport in 8 Mole Percent  $Y_{2}O_{3}$ - $ZrO_{2}$ . *J Electrochem Soc* 1989; **136**: 2867-2876.
- 7 Masó N, West AR. Electronic Conductivity in Yttria-Stabilized Zirconia under a Small *dc* Bias. *Chem Mater* 2015; **27**: 1552–1558.
- 8 Jovaní M, Beltrán-Mir H, Cordoncillo E, West AR. Atmosphere- and Voltage-Dependent Electronic Conductivity of Oxide-Ion-Conducting  $Zr_{1-x}Y_xO_{2-x/2}$

- Ceramics. *Inorg Chem* 2017; **56**: 7081–7088.
- 9 Masó N, Prades M, Beltrán H, Cordoncillo E, Sinclair DC, West AR. Field enhanced bulk conductivity of acceptor-doped  $\text{BaTi}_{1-x}\text{Ca}_x\text{O}_{3-x}$  ceramics. *Appl Phys Lett* 2010; **97**: 062907.
  - 10 Beltrán H, Prades M, Masó N, Cordoncillo E, West AR. Voltage-Dependent Low-Field Bulk Resistivity in  $\text{BaTiO}_3:\text{Zn}$  Ceramics. *J Am Ceram Soc* 2010; **93**: 500–505.
  - 11 Prades M, Masó N, Beltrán H, Cordoncillo E, West AR. Field enhanced bulk conductivity of  $\text{BaTiO}_3:\text{Mg}$  ceramics. *J Mater Chem* 2010; **20**: 5335.
  - 12 Masó N, Beltrán H, Prades M, Cordoncillo E, West AR. Field-enhanced bulk conductivity and resistive-switching in Ca-doped  $\text{BiFeO}_3$  ceramics. *Phys Chem Chem Phys* 2014; **16**: 19408–19416.
  - 13 Dong Y, Chen IW. Electrical and hydrogen reduction enhances kinetics in doped zirconia and ceria: II. Mapping electrode polarization and vacancy condensation in YSZ. *J Am Ceram Soc* 2018; **101**: 1058–1073.
  - 14 Cologna M, Rashkova B, Raj R. Flash sintering of nanograin zirconia in <5 s at 850°C. *J Am Ceram Soc* 2010; **93**: 3556–3559.
  - 15 Biesuz M, Sglavo VM. Flash sintering of ceramics. *J Eur Ceram Soc* 2019; **39**: 115–143.
  - 16 Yu M, Grasso S, McKinnon R, Saunders T, Reece MJ. Review of flash sintering: materials, mechanisms and modelling. *Adv Appl Ceram* 2016; **0**: 1–37.
  - 17 Cologna M, Prette ALG, Raj R. Flash-Sintering of Cubic Yttria-Stabilized Zirconia at 750°C for Possible Use in SOFC Manufacturing. *J Am Ceram Soc* 2011; **94**: 316–319.
  - 18 Yadav D, Raj R. The onset of the flash transition in single crystals of cubic zirconia as a function of electric field and temperature. *Scr Mater* 2017; **134**: 123–127.
  - 19 M’Peko JC, Francis JSC, Raj R. Impedance spectroscopy and dielectric properties of

- flash versus conventionally sintered yttria-doped zirconia electroceramics viewed at the microstructural level. *J Am Ceram Soc* 2013; **96**: 3760–3767.
- 20 M'Peko J-C, Francis JSC, Raj R. Field-assisted sintering of undoped BaTiO<sub>3</sub>: Microstructure evolution and dielectric permittivity. *J Eur Ceram Soc* 2014; **34**: 3655–3660.
- 21 ZHANG Y, NIE J, LUO J. Effects of phase and doping on flash sintering of TiO<sub>2</sub>. *J Ceram Soc Japan* 2016; **124**: 296–300.
- 22 Zapata-Solvas E, Bonilla S, Wilshaw PR, Todd RI. Preliminary investigation of flash sintering of SiC. *J Eur Ceram Soc* 2013; **33**: 2811–2816.
- 23 Sun K, Zhang J, Jiang T, Qiao J, Sun W, Rooney D *et al.* Flash-Sintering and Characterization of La<sub>0.8</sub>Sr<sub>0.2</sub>Ga<sub>0.8</sub>Mg<sub>0.2</sub>O<sub>3-δ</sub> Electrolytes for Solid Oxide Fuel Cells. *Electrochim Acta* 2016; **196**: 487–495.
- 24 Liu D, Cao Y, Liu J, Gao Y, Wang Y. Effect of oxygen partial pressure on temperature for onset of flash sintering 3YSZ. *J Eur Ceram Soc* 2018; **38**: 817–820.
- 25 Yoshida M, Falco S, Todd RI. Measurement and modelling of electrical resistivity by four-terminal method during flash sintering of 3YSZ. *J Ceram Soc Japan* 2018; **126**. doi:10.2109/jcersj2.17256.
- 26 Raj R. Joule heating during flash-sintering. *J Eur Ceram Soc* 2012; **32**: 2293–2301.
- 27 Hewitt IJ, Lacey AA, Todd RI. A Mathematical Model for Flash Sintering. *Math Model Nat Phenom* 2015; **10**: 77–89.
- 28 Terauds K, Lebrun JM, Lee HH, Jeon TY, Lee SH, Je JH *et al.* Electroluminescence and the measurement of temperature during Stage III of flash sintering experiments. *J Eur Ceram Soc* 2015; **35**: 3195–3199.
- 29 Biesuz M, Pinter L, Saunders T, Reece M, Binner J, Sglavo VM *et al.* Investigation of electrochemical, optical and thermal effects during flash sintering of 8YSZ. *Materials*

- (Basel) 2018; **11**. doi:10.3390/ma11071214.
- 30 Janek J, Korte C. Electrochemical blackening of yttria-stabilized zirconia - morphological instability of the moving reaction front. *Solid State Ionics* 1999; **116**: 181–195.
- 31 Thorp JS, Buckley HP. The dielectric constants of current- blackened single crystal yttria-stabilized zirconia. *J Mater Sci* 1973; **8**: 1401–1408.
- 32 Casselton RE. Blackening in yttria stabilized zirconia due to cathodic processes at solid platinum electrodes. *J Appl Electrochem* 1974; **4**: 25–48.
- 33 Bonola C, Camagni P, Chiodelli P, Samoggia G. Study of Defects Introduced by Electroreduction in YSZ. *Radiat Eff Defects Solids* 1991; **119–121**: 457–462.
- 34 Levy M, Fouletier J, Kleitz M. Model for the Electrical Conductivity of Reduced Stabilized Zirconia. *J Electrochem Soc* 1988; **135**: 1584.
- 35 Moghadam FK, Yamashita T, Stevenson DA. Characterization of the current-blackening phenomena in scandia stabilized zirconia using transmission electron microscopy. *J Mater Sci* 1983; **18**: 2255–2259.
- 36 Nazarpour S, Lopez C, Ramos F, Cirera A. Structural and electrical properties of Y-doped zirconia induced by electrical polarization. *Solid State Ionics* 2011; **184**: 19–22.

### Figure captions

**Figure 1.** Effect of the application of (A) 16 V (~70 V/cm), (B) 19 V (~80 V/cm) and (C) 24 V (~100 V/cm) to 8YSZ samples at 658 °C.

**Figure 2.** Impedance complex plane plots at 430 and 558 °C (inset) before and after different voltages are applied for 10 minutes.

**Figure 3.** Resistance at 558 °C as a function of time and atmosphere, on application and removal of 12 V (~50 V/cm) *dc* bias.

**Figure 4.** Experimental and fitted data for impedance complex plane plots and residuals at 430 °C before (a,c) and (b,d) after application of 12 V *dc* bias (~50 V/cm).

**Figure 5.** Transport number as a function of voltage applied at 558 °C.

**Figure 6.** Schematic ionic and electronic conductivity domains as a function of  $pO_2$ .